Cellular Uptake of Functional Nanogels Prepared by Inverse Miniemulsion ATRP with Encapsulated Proteins, Carbohydrates, and Gold Nanoparticles

ARTICLE *in* BIOMACROMOLECULES · JULY 2009

Impact Factor: 5.75 · DOI: 10.1021/bm9004904 · Source: PubMed

9 AUTHORS, INCLUDING:

Abiraman Srinivasan
Community College of Allegheny County
20 PUBLICATIONS **655** CITATIONS
SEE PROFILE

Sidi Bencherif
Harvard University
35 PUBLICATIONS **1,473** CITATIONS
SEE PROFILE

Anuradha Karunanidhi
University of Pittsburgh
8 PUBLICATIONS **80** CITATIONS
SEE PROFILE

Jung Kwon Oh
Concordia University Montreal
78 PUBLICATIONS **3,459** CITATIONS
SEE PROFILE

Cellular Uptake of Functional Nanogels Prepared by Inverse Miniemulsion ATRP with Encapsulated Proteins, Carbohydrates, and Gold Nanoparticles

Daniel J. Siegwart,[†] Abiraman Srinivasan,[‡] Sidi A. Bencherif,[†] Anuradha Karunanidhi,[‡] Jung Kwon Oh,[†] Swaroopa Vaidya,[‡] Rongchao Jin,[†] Jeffrey O. Hollinger,[‡] and Krzysztof Matyjaszewski*,[†]

Department of Chemistry, Carnegie Mellon University, 4400 Fifth Avenue, Pittsburgh, Pennsylvania 15213, and Bone Tissue Engineering Center, Carnegie Mellon University, 5000 Forbes Avenue, Pittsburgh, Pennsylvania 15213

Received April 27, 2009; Revised Manuscript Received June 6, 2009

Atom transfer radical polymerization (ATRP) was used to produce a versatile drug delivery system capable of encapsulating a range of molecules. Inverse miniemulsion ATRP permitted the synthesis of biocompatible and uniformly cross-linked poly(ethylene oxide)-based nanogels entrapping gold nanoparticles, bovine serum albumin, rhodamine B isothiocyanate-dextran, or fluoresceine isothiocyanate-dextran. These moieties were entrapped to validate several biological outcomes and to model delivery of range of molecules. Cellular uptake of nanogels was verified by transmission electron microscopy, gel electrophoresis, Western blotting, confocal microscopy, and flow cytometry. Fluorescent colocalization of nanogels with a fluorophore-conjugated antibody for clathrin indicated clathrin-mediated endocytosis. Furthermore, internalization of nanogels either with or without GRGDS cell attachment-mediating peptides was quantified using flow cytometry. After 45 min of incubation, the uptake of unmodified FITC-Dx-loaded nanogels was 62%, whereas cellular uptake increased to >95% with the same concentration of GRGDS-modified FITC-Dx nanogels. In addition, a spheroidal coculture of human umbilical vascular endothelial cells (HUVECs) and human mesenchymal stem cells (hMSCs) validated cell endocytosis. Application of ATRP enabled the synthesis of a functionalized drug delivery system with a uniform network that is capable of encapsulating and delivering inorganic, organic, and biological molecules.

Introduction

The development of effective polymer-based delivery systems is a key component of drug delivery, therapeutics, and imaging.[1,2] Because the properties of encapsulates vary considerably in size and chemical composition, a delivery system is needed that will universally deliver organic (e.g., drugs, dyes), inorganic (e.g., metals for imaging), and biological molecules (e.g., proteins, nucleic acids). Typically, customized polymer-based systems must be designed to encapsulate and match the properties of specific species. Herein, we describe a strategy that may alleviate customized systems by exploiting uniform nanogels capable of entrapping organic, inorganic, and biological molecules.

Microgels/nanogels[3−7] are an attractive class of delivery systems. The most common method for the preparation of well-defined microgel particles utilizes heterogeneous polymerization reactions of hydrophilic water-soluble monomers in the presence of either difunctional or multifunctional cross-linkers, including inverse (mini)emulsion polymerization.[8−14] Entrapment of drugs,[8,15,16] proteins,[9,14,17] and DNA[10,11,18] inside the polymeric network of microgels, as well as their release kinetics, have been investigated as targeted delivery carriers for biomedical applications.[19,20] Furthermore, it is known that delivery systems conjugated with biomolecules can recognize specific cell surface receptors and enable selective uptake.[9,14] Cell internalization is one of the key steps for effective delivery and controllable release of encapsulated molecules.

We recently developed a new method to synthesize nanogels that provides improved properties and unique features. Atom transfer radical polymerization (ATRP)[21−24] in inverse miniemulsion[25] was utilized to prepare functional cross-linked nanogels of well-controlled hydrophilic polymers. Because ATRP is a controlled radical polymerization (CRP) technique, monomers and cross-linkers incorporate in a regular fashion, and therefore yield polymer chains of equal length. The outcome is a uniform internal gel network, which is the crucial difference between nanogels prepared by ATRP and those prepared by conventional radical polymerization. We previously reported improved control over the release of encapsulated agents, swelling ratio, degradation, and colloidal stability for nanogels prepared by ATRP in inverse miniemulsion.[25,26]

The nanogel structure is based on poly(oligo(ethylene oxide) monomethyl ether methacrylate) (POEOMA), an analog of poly(ethylene glycol) (PEG), which may enhance the circulation time in the blood and prevent nanoparticle uptake by the reticuloendothelial system (RES).[27−29] We prepared nanogels loaded with doxorubicin (Dox), an anticancer drug, and demonstrated the utility of these nanogels as drug delivery carriers.[26] Due to incorporation of disulfide bonds into the network, the nanogels were biodegradable in a reducing environment to individual polymeric chains with narrow molecular weight distribution.

In this study, the three primary objectives were to (i) determine whether nanogels prepared by ATRP in inverse miniemulsion could be internalized into cells and, if so, to

* To whom correspondence should be addressed. E-mail: km3b@andrew.cmu.edu.
[†] Department of Chemistry.
[‡] Bone Tissue Engineering Center.

10.1021/bm9004904 CCC: $40.75
Published on Web 07/02/2009

elucidate the mechanism; (ii) functionalize nanogels with integrin-binding peptides to increase cellular uptake/attachment; and (iii) apply the ATRP system to encapsulate various biomolecules and inorganic species. To fulfill these objectives, nanogels were loaded in situ with rhodamine B isothiocyanate-labeled dextran (RITC-Dx), fluoresceine isothiocyanate-dextran (FITC-Dx), and bovine serum albumin (BSA) protein. Cell internalization of nanogels was confirmed by confocal microscopy, Western blotting, and flow cytometry. Covalent attachment of glycine-arginine-glycine-aspartic acid-serine (GRGDS) peptides to nanogels enhanced cell attachment/internalization. In addition, we extended the application range by encapsulating inorganic gold nanoparticles (AuNPs) because this strategy offers unique opportunities for applications in biology, catalysis, and nanotechnology.[30−32] For instance, photothermally driven volume transitions in polymer microgels with encapsulated AuNPs have promising applications for site-specific drug delivery and photodynamic therapy.[33] Thermogravimetric analysis (TGA) and transmission electron microscopy (TEM) demonstrated the encapsulation of AuNPs. These nanogels could also be internalized into cells. Finally, confocal microscopy showed that FITC-Dx-loaded nanogels could penetrate a coculture of human umbilical vein endothelial cells (HUVECs) and human mesenchymal stem cells (hMSCs) that mimicked complex tissue. These results confirmed that uniform nanogels prepared by ATRP in inverse miniemulsion are endocytosed and may be suitable for various drug delivery applications.

Experimental Section

Materials. Oligo(ethylene oxide) monomethyl ether methacrylate (OEOMA, MW = 300 g/mol) was purchased from Aldrich and purified by passage through a column filled with basic alumina to remove the inhibitor. Copper(II) bromide ($CuBr_2$, 99%), L-ascorbic acid (AscA, 99+%), sodium citrate, and 1-dodecanethiol were purchased from Acros and used without purification. Sorbitan monooleate (Span 80), poly(ethylene oxide) (PEO_{2000}, $M_{n,\,avg}$ = 2000), poly(ethylene glycol) (PEG) ($M_{n,\,avg}$ = 3400), cyclohexane (HPLC grade), rhodamine B isothiocyanate-dextran (RITC-Dx, MW = 40000, 0.002−0.01 mol RITC per mole of glucose), fluoresceine isothiocyanate-dextran (FITC-Dx, MW = 40000, 0.003−0.02 mol FITC per mole of glucose), tetrachloroauric(III) acid ($HAuCl_4 \cdot 3H_20$), chloroform, tetrahydrofuran (THF), and chloroform were purchased from Aldrich and used without purification. Tris[(2-pyridyl)methyl]amine (TPMA),[34,35] poly(ethylene oxide) dimethacrylate (PEO DMA, MW = 4600),[36] GRGDS PEG acrylate (MW = 3800),[37] and 2-hydroxyethyl 2-bromoisobutyrate (HO-EBiB)[38,39] were synthesized as described elsewhere.

Instrumentation. Molecular weights were determined by gel permeation chromatography (GPC) with THF as eluent at 35 °C at a flow rate of 1 mL/min and linear poly(methyl methacrylate) (PMMA) standards for calibration. The detailed GPC measurements were described elsewhere.[25] Conversion was also determined using GPC by following the decrease of the macromonomer peak area relative to the increase in the polymer peak area. Particle size and size distribution were measured by dynamic light scattering (DLS) in HPLC grade water or cyclohexane on a high performance particle sizer, Model HP5001 from Malvern Instruments, Ltd. The sizes are expressed as $D_{avg} \pm S$ (average diameter ± standard deviation). Optical fluorescence microscopy (OFM) was measured using a Zeiss Axiovert 200 microscope. Transmission Electron Microscopy (TEM) analysis was conducted using Hitachi H-7100 TEM. For the TEM measurements, a drop of dispersed nanogels was placed on a carbon grid. After several seconds, the drop was removed by blotting with filter paper. The sample that remained on the grid was allowed to dry before inserting the grid into the microscope. The mass change curves were recorded using a TA Instruments TGA 2950 thermogravimetric analyzer. Confocal imaging was performed on an Olympus FV1000 microscope. Fluorescence activated cell sorting (FACS) was performed using a Coulter Epix Elite flow cytometer from Beckman-Coulter.

Cell Culture. MC3T3-E4 mouse calvarial osteoprogenitor cells were obtained from American type Culture Collection and cultured in α-modified eagle medium (α-MEM), supplemented with 10% fetal bovine serum and 1% penicillin/streptomycin, all obtained from Invitrogen. Phalloidin-CY5 was obtained from Invitrogen. U-shaped 96-well tissue culture plates were obtained from Griener. FITC-conjugated Chicken anti-BSA was purchased from Gene Tex. Cell lysis buffer was purchased from Cell Signaling Technology. Mouse anti-clathrin FITC conjugate antibody was purchased from BD Biosciences. The micro bicinchoninic acid method and One-Step NBT/BCIP kit came from Pierce Biotechnology. Live/dead viability/cytotoxicity kit (Invitrogen), 35 mm diameter plates (BioFlex plate; Flexercell Corp.), and mesenchymal stem cell growth medium (Lonza) were also purchased. Human umbilical vein endothelial cells (HUVECs) were purchased from Clonetics and were maintained in endothelial cell growth medium. Human mesenchymal stem cells (hMSCs) were purchased from Poietics and maintained in mesenchymal stem cell medium (MSCGM).

Synthesis of Nanogels Loaded with RITC-Dx. Using a similar procedure to one previously reported,[40] stable nanogels containing RITC-Dx were prepared in the presence of RITC-Dx. In contrast to the previously published report, HO-EBiB instead of poly(ethylene oxide) (PEO)-functionalized 2-bromoisobutyrate (PEO_{2000}-Br),[41] was used to initiate the polymerization. A total of 1.4 g $OEOMA_{300}$ (4.67 mmol), 9.7 mg HO-EBiB (0.031 mmol), 0.572 g PEO DMA_{4600} (0.124 mmol), 50 mg PEO_{2000} (as a costabilizer), 70 mg RITC-Dx (5.0 wt. % of OEOMA), 3.5 mg $CuBr_2$ (0.016 mmol), 4.5 mg TPMA (0.016 mmol), and 1.4 mL of water were mixed in a 50 mL round-bottom flask at room temperature. The resulting translucent solution was mixed with a solution of 1.0 g Span 80 in 20.0 g cyclohexane, and the mixture was sonicated for 2 min in an ice bath at 0 °C to form a stable inverse miniemulsion. The dispersion was transferred into a 50 mL Schlenk flask and bubbled with nitrogen for 30 min. The flask was immersed in an oil bath preheated to 30 °C, and then a nitrogen-purged aqueous solution of AscA (181 μL of a deoxygenated 0.0946 mmol/mL solution in water, 0.017 mmol) was added dropwise over 2 min using a syringe to activate the catalyst and start the polymerization. The polymerization was stopped after 12 h by exposing the reaction mixture to air. A stable pink dispersion was obtained. The cross-linked nanogels were purified by addition of THF to the resulting dispersion, and then the resulting heterogeneous mixture was stirred at room temperature for 30 min. The nanogels were separated by centrifugation at 13000 rpm for 30 min at 4 °C. After the supernatant was removed, THF was added, and then the same procedure was repeated twice to completely remove THF-soluble species including unreacted monomer and surfactant. The isolated nanogels were dialyzed against water for 6 days, changing the water 12 times to purify the nanogels. A dialysis membrane with a 15000 MWCO was used, placed inside of a 1 L beaker filled with Millipore purified water.

Synthesis of Nanogels Loaded with FITC-Dx. The procedure for the synthesis of FITC-Dx-loaded nanogels was identical to the procedure for RITC-Dx-loaded nanogels except that 70 mg FITC-Dx (5.0 wt % of OEOMA) was added to the reaction mixture in the same manner described above.

Synthesis of GRGDS-Functionalized Nanogels Loaded with FITC-Dx. The procedure was identical to the procedure for FITC-Dx-loaded nanogels, except that 44.4 mg GRGDS-PEG-acrylate (0.012 mmol) was added to the reaction mixture in the same manner described above.

Synthesis of Nanogels Loaded with BSA. A total of 1.4 g $OEOMA_{300}$ (4.67 mmol), 9.7 mg HO-EBiB (0.031 mmol), 0.572 g PEO DMA_{4600} (0.124 mmol), 50 mg PEO_{2000} (as a costabilizer), 0.35 g BSA protein (25 wt %), and 1.4 mL water were added to a 25 mL vial. It was mixed thoroughly with the aid of a sonicator bath until a homogeneous solution resulted. A total of 3.5 mg $CuBr_2$ (0.016 mmol) and 4.5 mg TPMA (0.016 mmol) were added to a 50 mL round-bottom

wide-rimmed flask. The aqueous solution was then added to the flask containing the ligand and copper. It was mixed well until a fully homogeneous solution was obtained. Span 80 (1.0 g) and cyclohexane (20.0 g) were added to a 50 mL beaker and mixed well to combine. Then the surfactant/cyclohexane solution was added to the aqueous solution. It was sonicated for 2 min in an ice bath at 0 °C using a probe sonicator to form a stable inverse miniemulsion. The dispersion was transferred into a 50 mL Schlenk flask and bubbled with nitrogen for 30 min. The flask was immersed in an oil bath preheated to 30 °C, and then a nitrogen-purged aqueous solution of AscA (181 μL of a deoxygenated 0.0946 mmol/mL solution in water, 0.017 mmol) was added dropwise over 2 min using a syringe to activate the catalyst and start the polymerization. The polymerization was stopped after 12 h by exposing the reaction mixture to air. The cross-linked nanogels were purified by addition of THF to the resulting dispersion, and then the resulting heterogeneous mixture was stirred at room temperature for 30 min. The nanogels were separated by centrifugation at 13000 rpm for 30 min at 4 °C. The isolated nanogels were dialyzed against water for 7 days, changing the water 14 times to purify the nanogels. A dialysis membrane with a 12000 MWCO was used, placed inside of a 1 L beaker filled with Millipore purified water.

Synthesis of POEOMA Nanogels for AuNP Encapsulation. The synthetic procedure and purification by centrifugation and dialysis was identical to the experiments described above using the following amounts: 1.4 g $OEOMA_{300}$ (4.67 mmol), 9.7 mg HO-EBiB (0.031 mmol), 0.572 g PEO DMA_{4600} (0.124 mmol), 50 mg PEO_{2000} (as a costabilizer), 1.4 mL of water, 3.5 mg $CuBr_2$ (0.016 mmol), 4.5 mg TPMA (0.016 mmol), 1.0 g Span 80, 20.0 g cyclohexane, and AscA (181 μL of a deoxygenated 0.0946 mmol/mL solution in water, 0.017 mmol).

Synthesis of Gold Nanoparticles (AuNPs). $HAuCl_4$ (aq, 1.25 mL of 10 mM), sodium citrate (aq, 0.5 mL of 30 mM), and HS-$(CH_2)_{10}$-COONa (0.25 mL of 10 mM) were mixed with 50 mL of nanopure water (18.2 MΩ) in a 150 mL trineck round-bottom flask under constant magnetic stirring. The reaction system was briefly purged with N_2. Then, 1 mL of $NaBH_4$ aq solution (100 mM, freshly made with ice-cold nanopure water) was rapidly added into the solution under vigorous magnetic stirring. The solution color immediately turned from light yellow to dark brown, indicating the formation of small Au nanoparticles (approximately 2 nm in diameter, measured by TEM). The reaction was allowed to proceed for an additional 15 min. Then the colloid was transferred to a glass vial and stored either at room temperature or in a refrigerator prior to use.

Preparation of AuNP-Loaded Nanogels. Dried POEOMA nanogels (0.00245 g) were stirred in 25 mL of the AuNP solution ($\sim$0.25 mM) for two days. The contents were subsequently transferred to a dialysis bag with a membrane cutoff size of 12000−14000 Da. The mixture was dialyzed against water for 3 days, changing the water six times. To further separate any free AuNPs, the solution was filtered through a 100 nm membrane. The AuNP-loaded nanogels did not pass through the filter and were retained. The AuNP-loaded nanogels were recovered from the filter and the isolated composite was analyzed by TGA and used for cell culture experiments. Assuming 1.0 g of composite with the composition determined by TGA, the number of AuNPs per nanogel can be estimated, as follows: The number of gels (N_{nanogels}) should be equal to the mass of all of the nanogels divided by the mass of one nanogel $= m_{\text{all nanogels}}/m_{\text{one nanogel}} = m_{\text{all nanogels}}/(\rho \times (1/6) \times D^3 \times \pi) =$ 0.59 g/((1.0 $\times$ 10^{-21} g/nm^3) $\times$ (1/6) $\times$ (88 nm)^3 $\times$ π) = 1.65 $\times$ 10^{15} nanogels. Similarly, the number of AuNPs (N_{AuNPs}) can be calculated $= m_{\text{all AuNPs}}/m_{\text{one AuNP}} = m_{\text{all AuNPs}}/(\rho \times (1/6) \times D^3 \times \pi) = 0.41$ g/((19.3 $\times$ 10^{-21} g/nm^3) $\times$ (1/6) $\times$ (2 nm)^3 $\times$ π) = 5.07 $\times$ 10^{18} AuNPs. By comparing N_{AuNPs} to $N_{\text{nanoogels}}$ for 1.0 g of composite, there was an average of 3072 AuNPs inside of each nanogel. Based on a comparison of the volume of one nanogel to that of one AuNP, only 3.61% by volume of the AuNP-loaded nanogels is occupied by the AuNPs.

Sterilization of the Nanogels. A 20 mg/mL suspension of nanogels in sterile PBS was washed thoroughly, sterilized using 70% ethanol, and washed again thoroughly with sterile PBS to remove any residual ethanol. To recover the nanogels after every wash, the nanogels were centrifuged at 13000 rpm for 5 min and the supernatant was discarded. The nanogel pellet was washed with sterile incomplete media (α-MEM without FBS) and complete media (α-MEM with FBS) and then stored at 4 °C in suspension until being added to culturing cells.

Imaging of AuNP-Loaded Nanogels. MC3T3 cells (5 $\times$ 10^4) were seeded on 35 mm diameter membrane plates and were allowed to attach overnight. The following day, 900 μL of fresh cell culture media and 100 μL of AuNP-loaded nanogel suspension (2 mg/mL) were added to each well. Two sets of controls were performed, which received free AuNPs and no polymer/NPs. After 4, 8, and 24 h of incubation, the media was removed and the cells were washed with sterile PBS three times to remove cell culture media and any residual polymer. The cells were then fixed with 2.5% glutaraldehyde overnight, washed with sodium cacodylate buffer, postfixed with osmium tetroxide, dehydrated in ascending grades of alcohol, resin embedded in beam capsules, and allowed to polymerize at 60 °C. Ultrathin sections (100 nm) were cut using a Reichert-Jung Ultracut E Ultramicrotome and unstained sections were imaged by TEM.

Imaging of RITC-Dx-Loaded Nanogels. MC3T3-E1 (subclone 4) mouse calvarial osteoprogenitor cells were cultured in α-MEM, supplemented with 10% fetal bovine serum and 1% penicillin/streptomycin. MC3T3 cells (5 $\times$ 10^4) were incubated with 100 μL of a sterilized RITC-Dx-loaded suspension (2 mg/mL) in media for 24 h in a "U"-shaped bottom, nonadherent culture plate. The cells were collected and plated onto a glass coverslip and allowed to adhere to the surface. They were fixed with 2% paraformaldehyde, washed with PBS, counterstained with DAPI, and imaged using confocal microscopy. Confocal imaging was performed on an Olympus FV1000 microscope. All imaging conditions, including laser power, photomultiplier tube, and offset settings, remained constant for each comparison set. Each comparison set was also conducted during the same imaging period.

Imaging of RITC-Dx-Loaded Nanogels To Probe for Clathrin-Mediated Endocytosis. Mouse anticlathrin FITC conjugate antibody (1:100 dilution in PBS) was used to probe for clathrin-mediated endocytosis. Similar to the imaging experiment for RITC-Dx-loaded nanogels, the cells were fixed with 2% paraformaldehyde and permeabilized in 0.01% Triton X-100 and blocked for nonspecific binding with 1% BSA in PBS. The cells were then incubated with mouse anticlathrin FITC conjugate antibody 1:100 dilution in PBS for 1 h at room temperature in dark and washed thoroughly with PBS-Tween 20 to remove unbound antibodies and counter stained with DAPI and imaged using Olympus FV1000 confocal microscope.

Flow Cytometry. To measure the nanogel internalization efficiency, 4.5 $\times$ 10^5 MC3T3 cells were suspended in 1 mL of complete media for each sample. The control samples did not receive any polymer. Experimental samples received 500 μg of FITC-Dx-loaded nanogels (with and without GRGDS) from a fully homogeneous suspension. The vials were vortexed three times using 10 s pulses, and the contents of each tube were transferred to a nonadhesive U-shaped 96-well tissue culture plate and incubated for 45 or 90 min at 37 °C. The cells were collected into 1.5 mL centrifuge tubes and centrifuged at 2000 rpm for 3 min to pellet the cells. The supernatant was removed and the cells were resuspended in 1 mL of sterile PBS and transferred to FACS tubes. Each sample was analyzed using a Coulter Epix Elite flow cytometer. A total of 10000 events were recorded for each measurement.

Cytotoxicity. The BSA-loaded nanogels were tested for cell viability and cytotoxicity with MC3T3 cells using the Live/Dead cytotoxicity assay kit. A total of 5 $\times$ 10^4 cells/well were seeded in a 24-well tissue culture plate containing α-MEM, supplemented with 10% fetal bovine serum, 1% penicillin (100 units/mL), and streptomycin (100 μg/mL). To this, 100 μL of nanogel dispersed in culture media was added. The controls received 100 μL of PBS. After 24 and 48 h of culturing, the cell culture media was aspirated off, the culture wells were rinsed with PBS, and enough live/dead stain was added (calcein 1:2000 and ethidium homodimer 1:500, diluted in PBS). The cells were incubated

for 30 min at 37 °C in the dark and the images were captured using a monochrome CCD camera attached to a Zeiss Axiovert 200 microscope.

BSA Transfection. For BSA transfection studies, 5×10^4 MC3T3 cells were seeded directly onto the sterile coverslip in a 24-well plate and were allowed to attach overnight. The following day, 900 μL of fresh cell culture media was added to each well. To this, 100 μL of nanogel suspension containing BSA (2 mg/mL) was added. The positive controls were incubated with 1% BSA alone and the negative controls did not receive any nanogels or BSA. The internalization efficiency of the nanogels was assessed after 4, 6, 12, 24, and 48 h. Briefly, the cells were washed with PBS thoroughly to remove culture media and any residual polymer and fixed with 2% paraformaldehyde for 10 min and probed with FITC-conjugated chicken anti-BSA to detect the presence of BSA within the cells. To visualize the nucleus, the cells were counterstained using Hoechst blue (33258) and the images were captured using a monochrome CCD camera attached to a Zeiss Axiovert 200 microscope.

Western Blot of BSA-Loaded Nanogels. To prepare the cell lysate, cultures were terminated by aspirating the culture media and washed three times with ice-cold PBS and 500 μL of cell lysis buffer was added to the washed cells and incubated on ice for 15 min to solublize the cells. The cell lysate was harvested by scraping the culture plate and then transferred to microcentrifuge tubes and centrifuged at 13000 rpm for 20 min at 4 °C. The protein content of the clarified supernatant was determined by using the micro bicinchoninic acid method. Samples were normalized for protein concentration and subjected to SDS-PAGE and immunoblotting. To run the Western blot, samples were separated by SDS-PAGE under reducing conditions at constant voltage of 120 V for 1 h and proteins were transferred to nitrocellulose membranes at constant current of 0.35A. For immunoblottting, membranes were blocked in blocking buffer prior to the addition of the primary antibody (rabbit anti-BSA IgG) and overnight incubation at 4 °C with constant agitation. After three washes in Tris-buffered saline with 0.1% Tween for 5 min each, the immunoblots were incubated in secondary antibody (anti-rabbit IgG conjugated to alkaline phosphatase) for 45 min at room temperature on a rocker. The results were visualized by developing the immunoblots in One-Step NBT/BCIP that produces intense blue-purple signal when reacting with alkaline phosphatase. The Western blot image was analyzed for the percentage BSA transfection into cells, cultured in the presence of serum (+ serum) and in the absence of serum (− serum) using Optimas image analysis software (version 6.51).

Nanogel Transfection in Spheroidal Coculture Model. HUVECs and hMSCs were maintained in endothelial cell growth and mesenchymal stem cell growth medium. Carboxy methylcellulose (methocel) was prepared as previously described.[42−44] Subconfluent monolayers of HUVECs and hMSCs were trypsinized, counted, and equal amounts of HUVECs and hMSCs (2500 each) were suspended in methocel-containing medium (10% methocel stock solution, 90% mesenchymal stem cell culture medium). A total of 150 μL/well of cells was added to the U-shaped bottom, nonadhesive 96-well plates and cultured at 37 °C, supplemented with 5% CO_2 and 95% humidity. The suspended cells aggregated spontaneously within 4 h to form single coculture spheroid. The spheroids were harvested within 24 h and treated with FITC-Dx-loaded nanogels either with or without conjugated GRGDS peptides, the nuclei were DAPI-stained and the internalization efficiency was determined at 30 min, 1 h, and 2 h by confocal microscopy.

Results and Discussion

Synthesis and Confocal Imaging of RITC-Dx-Loaded Nanogels. Inverse miniemulsion ATRP enables the formation of uniformly cross-linked hydrophilic nanogels with control over molecular weight, molecular weight distribution, and functionality. In a previous report, we demonstrated effective encapsulation of RITC-Dx into POEOMA nanogels with up to 80% loading efficiency.[40] These nanogels were biocompatible and served as a model system for the loading and release of carbohydrate-based drugs. We also prepared nanogels loaded with Dox, an anticancer drug, and demonstrated the utility of these nanogels as drug delivery carriers.[26] Based on our previous results from assays of HeLa cancer cells,[26] the released Dox molecules suppressed the growth of cancer cells. However, it was unclear whether the Dox molecules were released into the cell cytoplasm after internalization or if the Dox was released into the surrounding media. Therefore, one objective of this study was to determine whether nanogels could penetrate cell membranes and be internalized and, if so, by what mechanism.

Table 1. Size of POEOMA Nanogels Measured by DLS and Expressed as Diameter ± Standard Deviation

entry	diameter (nm)
RITC-Dx-loaded POEOMA nanogels	151 ± 8
FITC-Dx-loaded POEOMA nanogels	110 ± 12
GRGDS-functionalized FITC-Dx-loaded POEOMA nanogels	115 ± 20
POEOMA nanogels (for AuNP encapsulation)	88 ± 9
BSA-loaded POEOMA nanogels	132 ± 8

In this report, inverse miniemulsion activator generated by electron transfer (AGET) ATRP of OEOMA in cyclohexane was utilized for the preparation of PEO DMA cross-linked POEOMA nanogels. HO-EBiB was used to initiate the ATRP inverse miniemulsion reactions, thereby providing a functional group that could be used for further bioconjugation.[45] Nanogels were synthesized using the conditions of $[OEOMA_{300}]_0/[HO\text{-}EBiB]_0/[PEO\ DMA_{4600}]_0/[CuBr_2]_0/[TPMA]_0/[ascorbic\ acid]_0 = 150/1/4//0.5/0.5/0.55$, $OEOMA_{300}$/water = 1/1 v/v, RITC-Dx = 5.0 wt % of $OEOMA_{300}$. In the absence of PEO DMA, droplets containing aqueous solutions of monomer become colloidal particles filled with swollen uncross-linked polymer chains. The resulting POEOMA was well controlled, with narrow molecular weight distribution ($M_w/M_n < 1.3$). In the presence of PEO DMA, the resulting particles were not soluble in any solvents, indicating that the particles were cross-linked during the polymerization. They had a narrow, monomodal size distribution of 151 ± 8 nm in diameter (Table 1). Microscope images of MC3T3 cells cultured with RITC-Dx-loaded POEOMA nanogel shows the containment of the RITC-Dx inside of the nanogels (Supporting Information, Figure S1).

To visualize internalization, confocal laser microscopy was employed to image RITC-Dx-loaded nanogels inside of cells. (Figure 1).

RITC-Dx-loaded nanogels enabled visualization of the nanogels inside of cells. Figure 1a shows the boundary of the cells. Nanogels are visualized as red spots within the cell boundary (Figure 1c). While a disulfide cross-linker was utilized previously[26] for triggered degradation, the purpose of this manuscript was to probe the internalization mechanism. Therefore, a PEO DMA cross-linker was employed because the macromolecular fluorophores could remain entrapped within the nanogels, allowing for clear visualization by confocal microscopy and analysis by flow cytometry.

Investigation of the Endocytotic Pathway. It has been shown that spherical particles with a diameter of 42−200 nm enter primarily via clathrin-coated pits.[46] Because our POEOMA nanogels are in that size range, we probed for clathrin-mediated endocytosis. After washing the cells to remove any residual noninternalized nanogels and serum proteins, the FITC-conjugated primary antibody for clathrin was added to detect clathrin. Clathrin is the major protein component of the vesicles formed during endocytosis. If the nanogels were endocytosized, then there should be a clathrin coating around the nanogels.

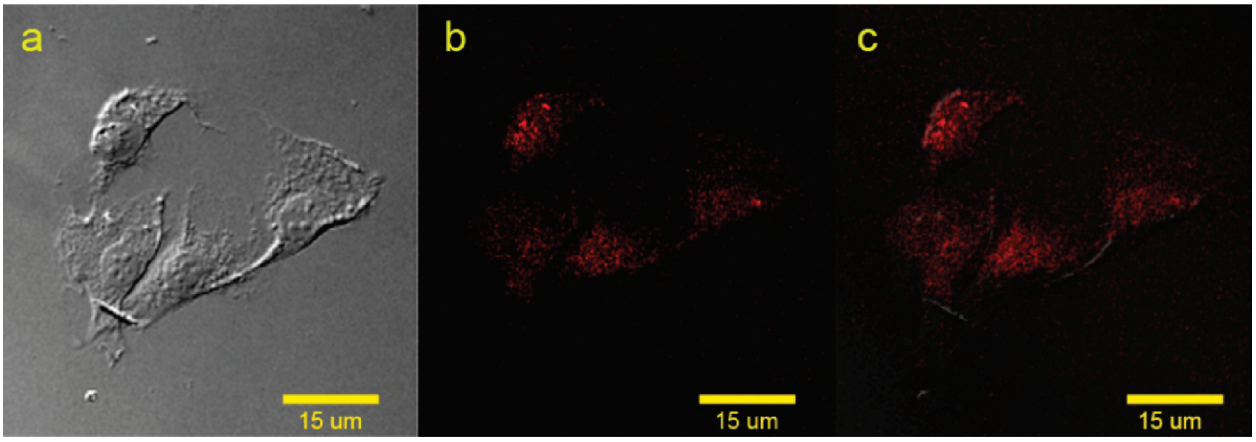

Figure 1. Confocal imaging of RITC-Dx-loaded nanogels. (a) Differential interference contrast (DIC), (b) fluorescence, and (c) merged DIC and fluorescence confocal images showing internalization of RITC-Dx-loaded nanogels after 24 h.

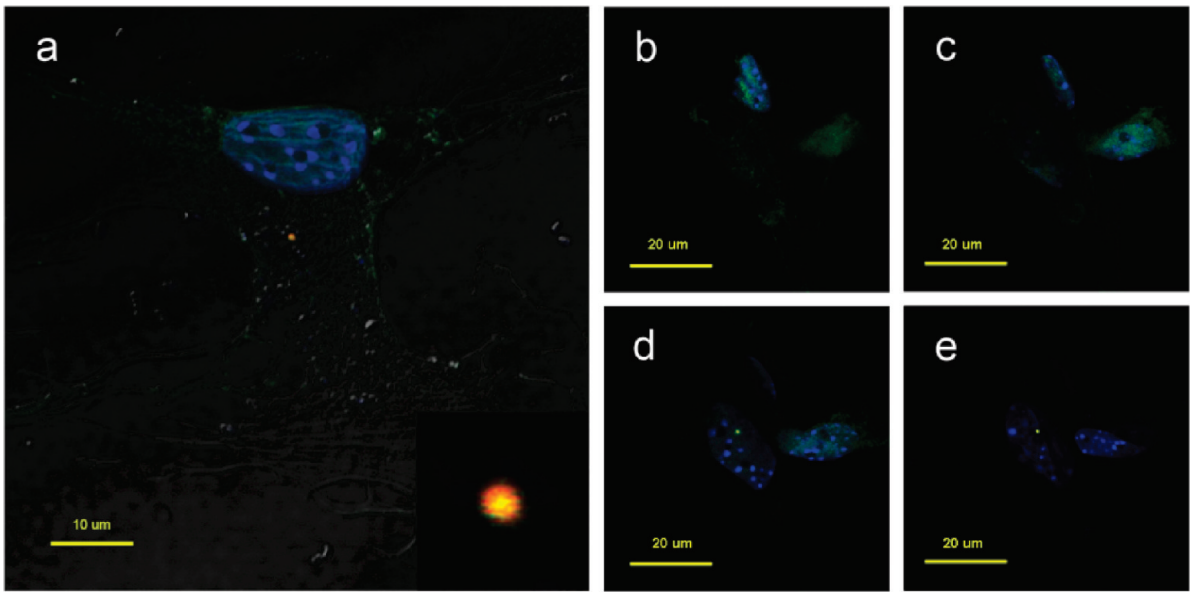

Figure 2. Clathrin-mediated endocytosis of RITC-Dx-loaded nanogels. (a) Combined fluorescent and DIC images of MC3T3 cells cultured with RITC-Dx-loaded POEOMA nanogels. Yellow colocalization of the red (RITC-Dx-loaded nanogels) and green (clathrin) signals indicates that there is a clathrin coating around the nanogels (see insert). Z-stack images (b−e) confirm that the nanogels are inside of the cells.

Combined florescence and DIC images appear in Figure 2. The structural outline of the cell can be visualized with the nucleus stained blue, the clathrin stained green, and the nanogels stained red. The yellow object in the middle of the cell is an aggregate of red RITC-Dx-loaded nanogels surrounded by a green clathrin coating. Colocalization of the red and green signals produces yellow, suggesting that some nanogels were internalized by clatharin-mediated endocytosis. A z-stack further suggests the presence of RITC-Dx-loaded nanogels within the cell, surrounded by clathrin (Figure 2b−e).

Quantification of Cell Internalization of FITC-Dx-Loaded Nanogels Using Flow Cytometry. Flow cytometry was utilized to measure the cell internalization or attachment of functional nanogels prepared by inverse miniemulsion ATRP. One of the key advantages of ATRP, compared to conventional radical polymerization methods for micro/nanogel formation is preserved end-functionality. We were therefore motivated to incorporate a cell attachment peptide into the nanogels and to compare the cell attachment/internalization to native nanogels. Nanogels containing a covalently attached peptide were prepared by copolymerizing POEOMA with an acrylate-terminated GRGDS peptide monomer. The ^{1}H NMR spectrum of the GRGDS-functionalized FITC-Dx-loaded POEOMA nanogels confirmed the covalent incorporation of the peptide into the cross-linked network (Figure S2). FITC-Dx-loaded POEOMA nanogels were synthesized with and without covalently attached GRGDS peptides. For comparison, nanogels of the same size were tested. The FITC-Dx-loaded nanogels were 110 nm in diameter (CV = 0.11), measured by DLS (Table 1). GRGDS-modified FITC-Dx-loaded nanogels were synthesized in parallel and the size was 115 nm (CV = 0.18). As described in the Experimental Section, MC3T3 cells were cultured in the presence of FITC-Dx-loaded POEOMA nanogels with and without covalently attached GRGDS. At different points, flow cytometry was used to quantify the intensity of FITC signal. Figure 3 presents count versus intensity plots and an illustration of the uniform network of the FITC-Dx-loaded GRGDS POEOMA nanogels.

The internalization (or attachment) of unmodified FITC-Dx-loaded nanogels was 62% after 45 min of incubation (yellow curve) and 95% after 45 min (at the same concentration of peptide-modified nanogels, green curve; Figure 3a). After 90 min, the cellular uptake increased to 82% for unmodified nanogels and 99% for peptide-modified nanogels, with a clean

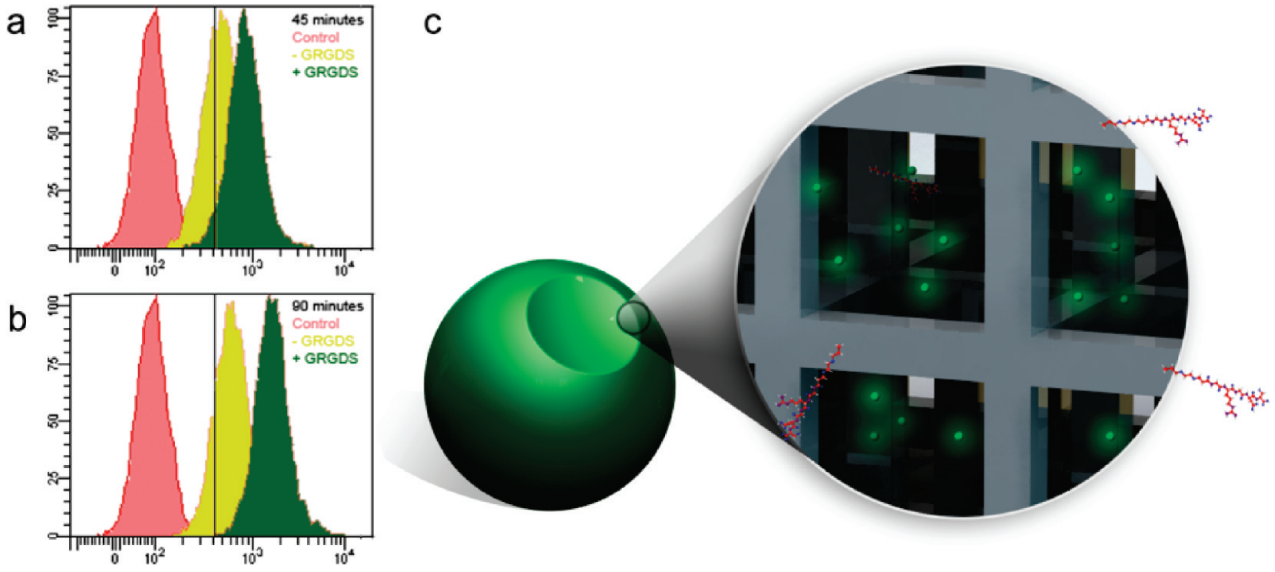

Figure 3. Flow cytometry results illustrating FITC fluorescence intensity for FITC-Dx-loaded POEOMA nanogels with and without covalently attached GRGDS at (a) 45 min and (b) 90 min. The inclusion of RITC-Dx molecules inside of the uniform POEOMA network (gray bars) functionalized with GRGDS is schematically illustrated in c.

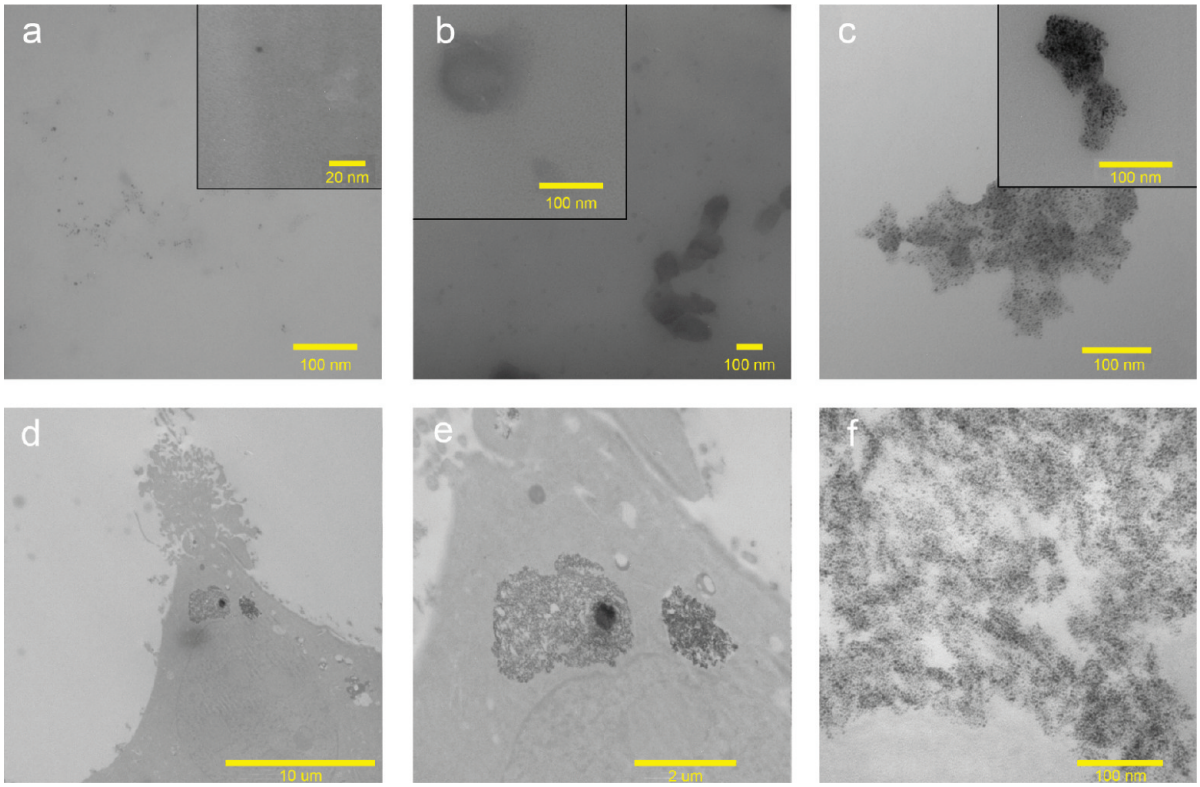

Figure 4. Formation and cellular uptake of AuNP-loaded nanogels. (a) Dispersed, free gold nanoparticles, (b) individual POEOMA nanogels, and (c) AuNP-POEOMA nanogel composites were imaged using TEM. After incubating the complex shown in (c) with MC3T3 cells, internalization of AuNP-loaded nanogels within the cells was observed on unstained sections (d−f). Parts d−f show the same area with increasing magnification.

shift toward higher fluorescence intensity (Figure 3b). FACS analysis of nanogels without FITC-Dx and of free GRGDS did not exhibit any fluorescent signal due to the absence of fluorescent markers.

A compelling advantage of ATRP is the tolerance to functional groups and capability for simple functionalization. This advantage was highlighted by synthesizing FITC-Dx nanogels for targeted delivery with covalently attached GRGDS by ATRP in inverse miniemulsion. Flow cytometry of cells cultured in the presence of these nanogels quantified the cellular association/uptake of the nanogels. At each time point, the peptide-modified nanogels more efficiently associated with the cells, demonstrating a higher internalization efficiency of the nanogels when mediated by a bioactive molecule.

Encapsulation of Gold Nanoparticles (Au-NPs) Inside POEOMA Nanogels and Verification of Cellular Uptake. Nanogels loaded with AuNPs could be used not only for verification of cell internalization but also for photodynamic therapy.[16,47] Figure 4a shows a TEM image of dispersed, free gold nanoparticles, deposited onto on a carbon grid. Individual

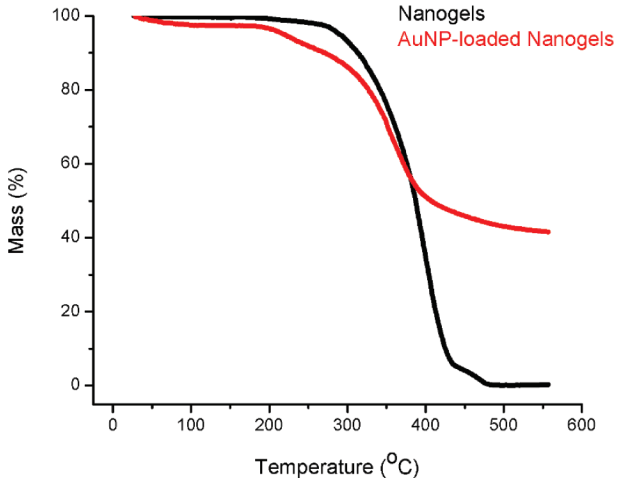

Figure 5. TGA plot showing percent mass loss versus temperature for the nanogels before and after entrapping the AuNPs.

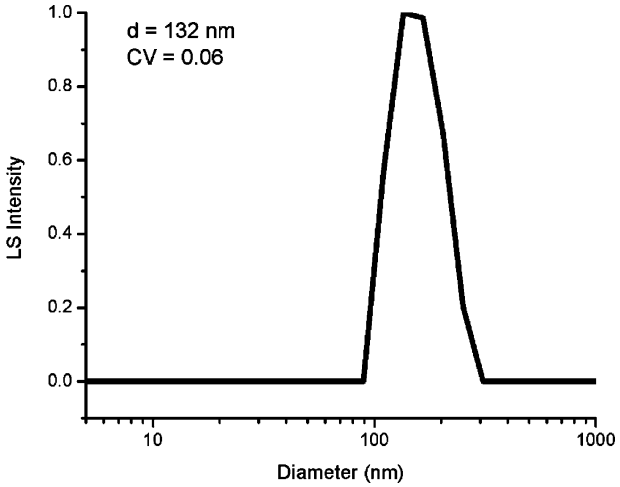

Figure 6. DLS plot of purified BSA-loaded POEOMA nanogels.

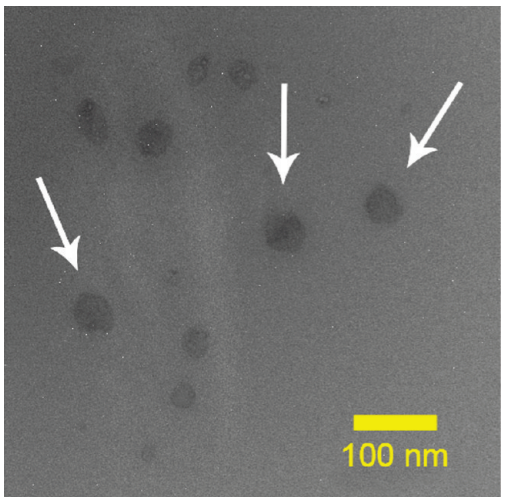

Figure 7. TEM image of purified BSA-loaded POEOMA nanogels, deposited onto a carbon grid.

POEOMA nanogels are presented in Figure 4b, where the insert contains a single POEOMA nanogel with a size around 90 nm. After encapsulation, AuNP-POEOMA nanogel composites were drop cast onto a carbon grid from water and imaged by TEM (Figure 4c). The AuNP nanogel composite inside of MC3T3 cells is presented in Figures 4d−f, which is the same area in increasing magnification. Figure 4d,e shows the cell membrane, and after zooming within the same area (Figure 4f), the clusters of AuNPs are observed within spherical POEOMA nanogels.

Based on TGA, each AuNP-loaded nanogel contained an approximately 3000 AuNPs, corresponding to 41% by mass or 3.6% by volume (Figure 5). Gold and silver nanoparticles have attracted interest in biomedicine. Stabilized nanoparticles[48,49] with functional properties[50,51] have been encapsulated in various ways.[52−54] However, a simple procedure to prepare encapsulated AuNPs remains challenging. Electron density contrast of POEOMA-based nanogels versus cells is not sufficient for TEM imaging and, consequently, AuNPs were incorporated into the nanogels to increase the electron density. The intracellular uptake of colloidal AuNPs with different sizes and shapes has been previously investigated.[55] Encapsulated AuNPs within polymer gels, however, should behave in a way different from bare AuNPs. AuNP-loaded nanogels were stable after dialysis and filtration. After 1 h, the AuNP-loaded nanogels were aggregated along the cell membrane and were not internalized (Figure S3). At later time points, the nanogels were endocytosed into the cells, as shown in Figure 4 and Figure S4. A high-resolution image of AuNP-loaded nanogels inside of cells confirms the lattice structure of the AuNPs (Figure S5). Control experiments were performed where free AuNPs and POEOMA nanogels were added at the same concentrations as the AuNP-loaded POEOMA nanogel experiment. However, the AuNPs could not be found within the samples. We deduce that the AuNPs were too small in comparison with the larger area of the cells to be efficiently recognized. The POEOMA nanogels were hidden by the cellular structures. These observations support the experimental design, aimed to enhance the TEM visibility of the nanogels via encapsulation of electron dense AuNPs.

Cytotoxicity and Cell Internalization of BSA-Loaded POEOMA Nanogels. Because we were able to prepare biocompatible nanogels loaded with macromolecular fluorophore-carbohydrates (RITC-Dx, and FITC-Dx), small organic molecules (Dox, R6G, as previously reported),[26] and inorganic AuNPs, we were interested in whether a protein could be encapsulated in situ and remain native following ATRP polymerization conditions, which involve transition metal halides complexed with amine ligands and heating.

To prepare nanogels entrapped with a protein, BSA was added into the aqueous solution consisting of OEOMA, HO-EBiB, $CuBr_2$/TPMA, PEO DMA, and water. The resulting transparent solution was mixed with the organic solution of Span 80 in cyclohexane. This mixture was sonicated in an ice-bath at 0 °C to form stable inverse miniemulsion of monomer droplets. An aqueous AscA solution was added to start polymerization, resulting in cross-linked POEOMA particles containing BSA.

DLS measurements showed the size of the particles to be on average 132 nm in diameter with narrow size distribution (Figure 6). A slightly smaller size was observed after dropping a suspension of the nanogels onto a carbon grid and imaging by TEM (Figure 7). This is likely due to blotting off the excess water using filter paper, which caused some contraction of the nanogels on the hydrophobic carbon grid.

The cytotoxicity of BSA-loaded nanogels was measured by the live/dead cell assay. The live and dead cell determination indicated 95 ± 1% viability of MC3T3 cells in the presence of nanogels compared to 96 ± 1% viability of MC3T3 cells in the controls, where no nanogels were added (Figure S6). These results suggested that BSA-loaded nanogels of POEOMA prepared by inverse miniemulsion ATRP were nontoxic and that

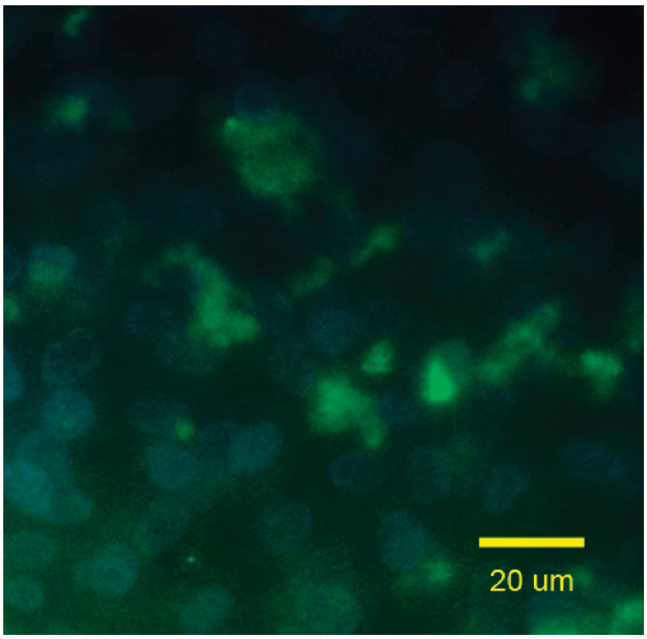

Figure 8. Fluorescence microscopy image of MC3T3 cells after 6 h incubation with BSA-loaded nanogels showed green BSA proteins due to the recognition of BSA by the FITC-conjugated antibody for BSA and blue nuclei stained with Hoechst.

polymers prepared by ATRP can be easily purified for biological applications.

BSA activity was determined after the in situ ATRP polymerization to investigate whether the protein denatured. A FITC-conjugated anti-BSA primary antibody was utilized to confirm the cellular uptake of BSA into the cells. The locations of BSA proteins within the cells were identified as a green color (Figure 8). After 6 h of incubation, more than 60% of cells showed BSA positive staining. Control experiments with free BSA showed significantly less positive staining (Figure S7). Therefore, BSA can be encapsulated into the nanogels in situ and at least some of the protein remains native after polymerization. Furthermore, a Western blot (Figure 9) of lysed cells confirmed the presence of BSA-loaded nanogels inside of the cells. The "(−) serum" label indicates that the cells were deprived of the serum normally present in the medium. Because BSA from the medium may affect the signal from the cells containing BSA-loaded nanogels, serum starvation was used to differentiate BSA protein signal coming from the nanogels within the cells. Lanes 5, 6, and 7 are labeled as (+) serum, indicating that the cells were under normal serum (10% FBS) conditions. The immunoblot reveals that, in serum starved and normal serum conditions, there is more BSA signal in cells loaded with BSA-containing nanogels compared to cells alone. The percentage of internalization was quantified using densitometric analysis of the immunoblot. In serum-starved conditions, 35.3% internalization was measured for the BSA-loaded nanogels, compared to 15.4% BSA measured in the control. The results therefore suggest that the BSA-loaded nanogels were internalized into the cells.

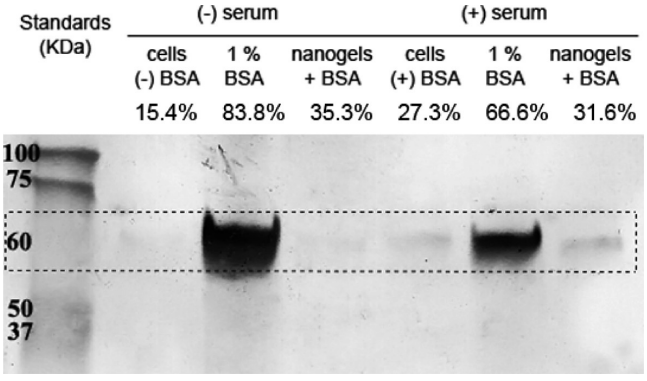

Figure 9. Western blot of MC3T3 cell extracts cultured with and without BSA-loaded nanogels verified internalization. The percentage of BSA internalization was quantified using densitometric analysis.

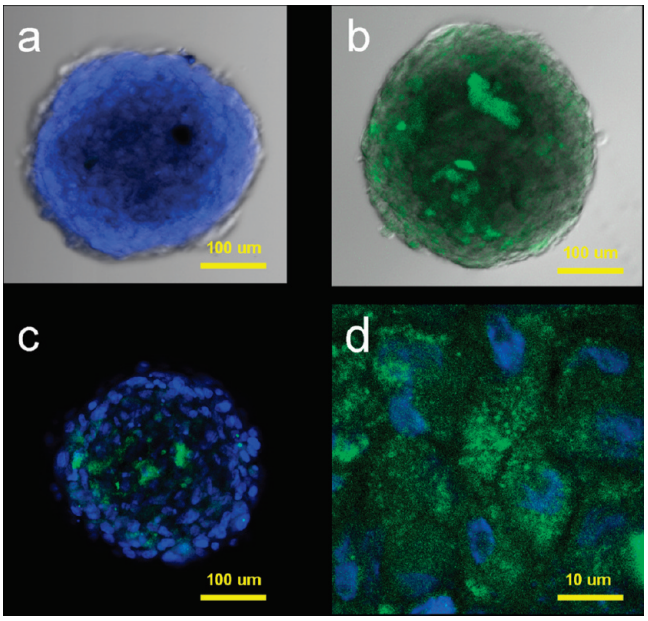

Figure 10. Spheroidal coculture model. Merged DIC and fluorescent confocal images of a control (a) spheroid and one cultured with FITC-Dx-loaded nanogels for 1 h (b). Confocal images of spheroids cultured in the presence of FITC-Dx-loaded nanogels without GRGDS (c) and with GRGDS (d) after 2 hrs. The optical section shown in d was taken at 28 μm cell depth into the coculture spheroid.

Spheroidal Coculture Model in the Presence of FITC-Dx-Loaded Nanogels. The in vitro data suggests that nanogels prepared by inverse miniemulsion ATRP can enter cells; however, the in vivo environment presents more challenging conditions for delivery. Therefore, to more closely capture an in vivo environment than typically encountered in a single phenotype 2D tissue culture system, we used a 3D coculture of hMSC and HUVEC spheroids. FITC-Dx-loaded nanogels with and without GRGDS peptide were taken into the coculture spheroids with high efficiency (Figure 10).

Endothelial cells line the inside of blood vessels as an epithelioid monocellular layer.[56] Correspondingly, endothelial cells can be grown on tissue culture surfaces to form a monocellular layer that mimics many of the phenotypic and functional properties of endothelial cells in vivo.[57,58] Nanogels were cultured with the spheroids to evaluate if they could penetrate the cell cluster. This coculture environment served as an in vitro model composed of different cell types arranged to mimic tissue with a multitude of growth factors and processes present.

The outcome of the 3D spheroidal coculture of hMSCs and HUVECs was that FITC-Dx-loaded nanogels penetrated the cell cluster with high efficiency, demonstrated by the abundance of FITC signal in the confocal images (Figure 10b−d). Additional optical sections into the coculture spheroid with internalized GRGDS FITC-Dx nanogels are presented in Figure S8. The control spheroid without added nanogels did not exhibit such

fluorescence (Figure 10a), indicting that the nanogels could be taken into the coculture spheroids and are applicable to deliver molecules inside of complex tissue.

Conclusion

Biocompatible nanogels were prepared by in situ entrapment of RITC-Dx, FITC-Dx, BSA, and AuNPs, using ATRP in cyclohexane−water inverse miniemulsion. The nanogels consisted of POEOMA, an analog of linear PEO which can prevent nanoparticle uptake by reticuloendothelial system. The nanogels were cross-linked using PEO DMA and initiated by a hydroxyl-functionalized initiator. Optionally, they were covalently conjugated with a GRGDS peptide sequence for targeted delivery. Confocal imaging of RITC-Dx-loaded nanogels demonstrated that the nanogels were internalized, and the location of the nanogels was confirmed by staining for actin and nuclei, as well as by following along the *z*-axis. Furthermore, colocalization of the RITC signal with a signal for a FITC-conjugated antibody for clathrin indicated that the nanogels enter via clathrin-mediated endocytosis. The internalization of FITC-Dx-loaded nanogels with and without GRGDS into cells was quantified using flow cytometry and exceeded 95%. Cell uptake of AuNP-loaded nanogels was verified using TEM. Cell internalization of BSA-loaded nanogels was confirmed using fluorescence microscopy after the addition of a fluorescently tagged antibody for BSA, and by running a Western blot of the cell extracts. The in vitro cell work confirmed that uniform nanogels prepared by ATRP in inverse miniemulsion are endocytosed and could serve as drug delivery devices.

Acknowledgment. The authors gratefully acknowledge Professor Simon Watkins (Center for Biologic Imaging, University of Pittsburgh School of Medicine) for access to the confocal microscope, Glenn Papworth and Greg Gibson for operating the confocal microscope, Professor Alan Waggoner (Molecular Biosensor and Imaging Center, Carnegie Mellon University) for access to the flow cytometer, Yehuda Creeger for operating the flow cytometer, Dr. Joseph Suhan for preparing and imaging the TEM samples, Tom Nuhfer for taking the high resolution TEM image, and Dr. Wei Wu for running the TGA. Robert S. Siegwart is acknowledged for graphical assistance. Hongchen Dong and Dr. Andrew K. Bohaty are acknowledged for useful discussions. Support came from the CRP Consortium at Carnegie Mellon University, the National Science Foundation Grant DMR-0549353, the National Tissue Engineering Center Grant DAMA 17-02-0717, and the National Institutes of Health Grant NIH RO1 DE15392 (J.O.H.).

Supporting Information Available. Additional microscopy images, ^{1}H NMR spectra of nanogels with and without attached GRGDS, and additional TEM images of internalized AuNP-loaded nanogels appear in Figures S1−S8. This material is available free of charge via the Internet at http://pubs.acs.org.

References and Notes

(1) Duncan, R. *Nat. Rev. Drug Discovery* **2003**, *2*, 347–360.
(2) (a) Langer, R. *Science* **2001**, *293*, 58–59. (b) Dandu, R.; Ghandehari, H. *Prog. Polym. Sci.* **2007**, *32*, 1008–1030. (c) Deming, T. J. *Prog. Polym. Sci.* **2007**, *32*, 858–875. (d) Discher, D. E.; Ortiz, V.; Srinivas, G.; Klein, M. L.; Kim, Y.; Christian, D.; Cai, S.; Photos, P.; Ahmed, F. *Prog. Polym. Sci.* **2007**, *32*, 838–857. (e) Hoffman, A. S.; Stayton, P. S. *Prog. Polym. Sci.* **2007**, *32*, 922–932. (f) Kabanov, A. V.; Gendelman, H. E. *Prog. Polym. Sci.* **2007**, *32*, 1054–1082. (g) Jeong, J. H.; Kim, S. W.; Park, T. G. *Prog. Polym. Sci.* **2007**, *32*, 1239–1274. (h) Kim, J.-H.; Park, K.; Nam, H. Y.; Lee, S.; Kim, K.; Kwon, I. C. *Prog. Polym. Sci.* **2007**, *32*, 1031–1053. (i) Kumar, A.; Srivastava, A.; Galaev, I. Y.; Mattiasson, B. *Prog. Polym. Sci.* **2007**, *32*, 1205–1237. (j) Lee, K. Y.; Yuk, S. H. *Prog. Polym. Sci.* **2007**, *32*, 669–697. (k) Nair, L. S.; Laurencin, C. T. *Prog. Polym. Sci.* **2007**, *32*, 762–798. (l) Pasut, G.; Veronese, F. M. *Prog. Polym. Sci.* **2007**, *32*, 933–961. (m) Rapoport, N. *Prog. Polym. Sci.* **2007**, *32*, 962–990. (n) Vert, M. *Prog. Polym. Sci.* **2007**, *32*, 755–761. (o) Wong, S. Y.; Pelet, J. M.; Putnam, D. *Prog. Polym. Sci.* **2007**, *32*, 799–837. (p) Yamato, M.; Akiyama, Y.; Kobayashi, J.; Yang, J.; Kikuchi, A.; Okano, T. *Prog. Polym. Sci.* **2007**, *32*, 1123–1133. (q) Bajpai, A. K.; Shukla, S. K.; Bhanu, S.; Kankane, S. *Prog. Polym. Sci.* **2008**, *33*, 1088–1118. (r) Lutz, J.-F.; Boerner, H. G. *Prog. Polym. Sci.* **2008**, *33*, 1–39. (s) Park, J. H.; Lee, S.; Kim, J.-H.; Park, K.; Kim, K.; Kwon, I. C. *Prog. Polym. Sci.* **2008**, *33*, 113–137. (t) Venkatraman, S.; Boey, F.; Lao, L. L. *Prog. Polym. Sci.* **2008**, *33*, 853–874.
(3) Langer, R.; Peppas, N. A. *AIChE J.* **2003**, *49*, 2990–3006.
(4) Hoffman, A. S. *J. Controlled Release* **1987**, *6*, 297–305.
(5) Sahiner, N.; Godbey, W. T.; McPherson, G. L.; John, V. T. *Colloid Polym. Sci.* **2006**, *284*, 1121–1129.
(6) Oh, J. K.; Drumright, R.; Siegwart, D. J.; Matyjaszewski, K. *Prog. Polym. Sci.* **2008**, *33*, 448–477.
(7) Murthy, N.; Thng, Y. X.; Schuck, S.; Xu, M. C.; Fréchet, J. M. J. *J. Am. Chem. Soc.* **2002**, *124*, 12398–12399.
(8) Missirlis, D.; Tirelli, N.; Hubbell, J. A. *Langmuir* **2005**, *21*, 2605–2613.
(9) Kwon, Y. J.; Standley, S. M.; Goh, S. L.; Fréchet, J. M. J. *J. Controlled Release* **2005**, *105*, 199–212.
(10) Goh, S. L.; Murthy, N.; Xu, M.; Fréchet, J. M. J. *Bioconjugate Chem.* **2004**, *15*, 467–474.
(11) McAllister, K.; Sazani, P.; Adam, M.; Cho, M. J.; Rubinstein, M.; Samulski, R. J.; DeSimone, J. M. *J. Am. Chem. Soc.* **2002**, *124*, 15198–15207.
(12) Braun, O.; Selb, J.; Candau, F. *Polymer* **2001**, *42*, 8499–8510.
(13) Craparo, E. F.; Cavallaro, G.; Bondi, M. L.; Mandracchia, D.; Giammona, G. *Biomacromolecules* **2006**, *7*, 3083–3092.
(14) Murthy, N.; Xu, M.; Schuck, S.; Kunisawa, J.; Shastri, N.; Fréchet, J. *Proc. Natl. Acad. Sci. U.S.A.* **2003**, *100*, 4995–5000.
(15) Zhang, H.; Mardyani, S.; Chan, W. C. W.; Kumacheva, E. *Biomacromolecules* **2006**, *7*, 1568–1572.
(16) Das, M.; Mardyani, S.; Chan, W. C. W.; Kumacheva, E. *Adv. Mater.* **2006**, *18*, 80–83.
(17) Nolan, C. M.; Gelbaum, L. T.; Lyon, L. A. *Biomacromolecules* **2006**, *7*, 2918–2922.
(18) Yun, Y. H.; Goetz, D. J.; Yellen, P.; Chen, W. *Biomaterials* **2003**, *25*, 147–157.
(19) Qi, K.; Ma, Q.; Remsen, E. E.; Clark, C. G., Jr.; Wooley, K. L. *J. Am. Chem. Soc.* **2004**, *126*, 6599–6607.
(20) Hawker, C. J.; Wooley, K. L. *Science* **2005**, *309*, 1200–1205.
(21) Matyjaszewski, K.; Xia, J. *Chem. Rev.* **2001**, *101*, 2921–2990.
(22) Kamigaito, M.; Ando, T.; Sawamoto, M. *Chem. Rev.* **2001**, *101*, 3689–3745.
(23) Wang, J.-S.; Matyjaszewski, K. *J. Am. Chem. Soc.* **1995**, *117*, 5614–15.
(24) Tsarevsky, N.; Matyjaszewski, K. *Chem. Rev.* **2007**, *107*, 2270–2299.
(25) Oh, J. K.; Tang, C.; Gao, H.; Tsarevsky, N. V.; Matyjaszewski, K. *J. Am. Chem. Soc.* **2006**, *128*, 5578–5584.
(26) Oh, J. K.; Siegwart, D. J.; Lee, H. I.; Sherwood, G.; Peteanu, L.; Hollinger, J. O.; Kataoka, K.; Matyjaszewski, K. *J. Am. Chem. Soc.* **2007**, *129*, 5939–5945.
(27) Seymour, L. W.; Duncan, R.; Strohalm, J.; Kopecek, J. *J. Biomed. Mater. Res., Part A* **1987**, *21*, 1341–58.
(28) Nishiyama, N.; Kataoka, K. *Adv. Polym. Sci.* **2006**, *193*, 67–101.
(29) Harada, A.; Kataoka, K. *Prog. Polym. Sci.* **2006**, *31*, 949–982.
(30) Daniel, M. C.; Astruc, D. *Chem. Rev.* **2004**, *104*, 293–346.
(31) Zhang, J.; Xu, S.; Kumacheva, E. *J. Am. Chem. Soc.* **2004**, *126*, 7908–7914.
(32) Pich, A.; Karak, A.; Lu, Y.; Ghosh, A. K.; Adler, H. J. P. *J. Nanosci. Nanotech.* **2006**, *6*, 3763–3769.
(33) Das, M.; Sanson, N.; Fava, D.; Kumacheva, E. *Langmuir* **2007**, *23*, 196–201.
(34) Tyeklar, Z.; Jacobson, R. R.; Wei, N.; Murthy, N. N.; Zubieta, J.; Karlin, K. D. *J. Am. Chem. Soc.* **1993**, *115*, 2677–89.
(35) (a) Xia, J.; Matyjaszewski, K. *Macromolecules* **1999**, *32*, 2434–2437. (b) Pintauer, T.; Matyjaszewski, K. *Coord. Chem. Rev.* **2005**, *249*, 1155–1184.

(36) Lin-Gibson, S.; Bencherif, S.; Cooper, J. A.; Wetzel, S. J.; Antonucci, J. M.; Vogel, B. M.; Horkay, F.; Washburn, N. R. *Biomacromolecules* **2004**, *5*, 1280–1287.
(37) Siegwart, D.; Bencherif, S.; Srinivasan, A.; Hollinger, J.; Matyjaszewski, K. *J. Biomed. Mater. Res., Part A* **2008**, *87A*, 345–358.
(38) Sarbu, T.; Lin, K.-Y.; Spanswick, J.; Gil, R. R.; Siegwart, D. J.; Matyjaszewski, K. *Macromolecules* **2004**, *37*, 9694–9700.
(39) Coessens, V.; Matyjaszewski, K. *Macromol. Rapid Commun.* **1999**, *20*, 127–134.
(40) Oh, J. K.; Siegwart, D. J.; Matyjaszewski, K. *Biomacromolecules* **2007**, *8*, 3326–3331.
(41) Oh, J. K.; Min, K.; Matyjaszewski, K. *Macromolecules* **2006**, *39*, 3161–3167.
(42) Alon, T.; Hemo, I.; Itin, A.; Pe'er, J.; Stone, J.; Keshet, E. *Nat. Med.* **1995**, *1*, 1024–1028.
(43) Korff, T.; Augustin, H. G. *J. Cell Biol.* **1998**, *143*, 1341.
(44) Korff, T.; Kimmina, S.; Martiny-Baron, G.; Augustin, H. G. *FASEB J.* **2001**, *15*, 447–457.
(45) Siegwart, D.; Oh, J.; Gao, H.; Bencherif, S.; Perineau, F.; Bohaty, A.; Hollinger, J.; Matyjaszewski, K. *Macromol. Chem. Phys.* **2008**, *209*, 2180–2193.
(46) Lai, S. K.; Hida, K.; Man, S. T.; Chen, C.; Machamer, C.; Schroer, T. A.; Hanes, J. *Biomaterials* **2007**, *28*, 2876–2884.
(47) Das, M.; Sanson, N.; Fava, D.; Kumacheva, E. *Langmuir* **2007**, *23*, 196–201.
(48) Burda, C.; Chen, X. B.; Narayanan, R.; El-Sayed, M. A. *Chem. Rev.* **2005**, *105*, 1025–1102.
(49) Khanal, B. P.; Zubarev, E. R. *Angew. Chem., Int. Ed.* **2007**, *46*, 2195–2198.
(50) Sato, T.; Ahmed, H.; Brown, D.; Johnson, B. F. G. *J. Appl. Phys.* **1997**, *82*, 696–701.
(51) Elghanian, R.; Storhoff, J. J.; Mucic, R. C.; Letsinger, R. L.; Mirkin, C. A. *Science* **1997**, *277*, 1078–1081.
(52) Gao, X. H.; Cui, Y. Y.; Levenson, R. M.; Chung, L. W. K.; Nie, S. M. *Nat. Biotechnol.* **2004**, *22*, 969–976.
(53) Dubertret, B.; Skourides, P.; Norris, D. J.; Noireaux, V.; Brivanlou, A. H.; Libchaber, A. *Science* **2002**, *298*, 1759–1762.
(54) Doering, W. E.; Nie, S. M. *Anal. Chem.* **2003**, *75*, 6171–6176.
(55) Chithrani, B. D.; Ghazani, A. A.; Chan, W. C. W. *Nano Lett.* **2006**, *6*, 662–668.
(56) Alon, T.; Hemo, I.; Itin, A.; Peer, J.; Stone, J.; Keshet, E. *Nat. Med.* **1995**, *1*, 1024–1028.
(57) Korff, T.; Augustin, H. G. *J. Cell Biol.* **1998**, *143*, 1341–1352.
(58) Korff, T.; Kimmina, S.; Martiny-Baron, G.; Augustin, H. G. *FASEB J.* **2001**, *15*, 447–457.

BM9004904